Deformations of CMP Gathers With $\bar{v}(z)$ To Hyperbolas

Alfonso González-Serrano
Jon F. Claerbout

Abstract

Mapping Snell-traces to Radial-traces, using an approximate velocity function $\bar{v}(z)$ into ray-tracing equations, provides a practical way of stretching reflection events to hyperbolas, increasing resolution of the velocity-spectrum in *CMP* gathers.

Conventional velocity analysis

Velocity estimation represents an important step in seismic data-processing. The most widely adopted process to obtain a *velocity−spectrum* has been described by Tanner and Koehler (1969). We refer to this process as *conventional*. The success of this process is due mainly on two facts: its ease of computation, and the quasi-hyperbolicity of reflection events in *CMP* gathers for near offsets. When these conditions are satisfied, the resolution of the method is close to the velocity information content of the data.

With high resolution seismic-data, which usually comprises a wide range of offsets, plus a dense sampling in time, the assumption of hyperbolicity in the data can severly limit the quality of the *conventional* velocity-spectrum. This problem is most critical when there is a well defined (sharp) discontinuity between two formations. For instance the sea-bottom and sediments below. It follows that arrival times for reflection events close to the discontinuity will refract significantly, violating the straight-ray assumption required by the conventional method. On the other hand it is these reflection events, the ones close to the sea floor, that are usually the most important in geophysical prospecting. Also it is for these events that we have a the widest range of angles in the recorded data. It follows that for these events we demand the most resolution in the velocity estimation process.

Non-hyperbolic velocity estimators

Several methods have been presented in the literature to deal with the problem of non-hyperbolicity of reflection events in *common midpoint*, (*CMP*) gathers. They can be grouped in two categories. First, methods that use higher-order terms in the series expansion of traveltime as function of offset (Bruce and Straley, 1979). This approach requires a search for the velocity function in a $3-D$ space. In a practical implementation we still need to assume quadratic approximations for the traveltime equation, this way we can start by searching for the quadratic term in $2-D$ space, subsequently correcting for higher order terms. Second, methods that use an estimated velocity function $\bar{v}(z)$ into either the wave equation (González and Claerbout, 1979, SEP-16, p. 181-204), or the ray-tracing equations. The method we propose in this paper belongs to this last category. Wave equation velocity estimation is still a subject of research.

Transformation to radial-trace space

If we take a *CMP* gather from an stratified earth model, the trajectory followed by a *Snell wave* (see Claerbout, 1978, SEP-15, p. 57-71) with fixed Snell parameter p defines a *Snell trace*. If the earth model has constant velocity, then the Snell trace becomes an straight line with slope dt/dh, where h refers to half-offset. We call this straight line trace a *Radial trace*. We refer the reader to Ottolini's paper (this SEP volume), where he discusses the properties of both Snell traces and Radial traces in detail.

We may think of a process that takes *CMP* data into radial trace space using some estimation for the stratified-earth velocity model $\bar{v}(z)$, next transforming back to *CMP* data. This last step is done replacing the velocities of the depth-model with a constant mapping velocity $\hat{v}$. Reflection events in the new *CMP* data should be close to hyperbolas, and conventional velocity estimation should give better resolution.

To stretch a Snell trace into radial trace domain we have two options. Either, we may want to maintain the *arrival times* invariant, doing the transformation by stretching depth-offset coordinates, or we may want to maintain the *depth* model invariant, doing the transformation by stretching time-offset coordinates. See Ottolini (this SEP volume) for a discussion of the first alternative. We approach the second alternative.

Another perspective to the same process would be to use the double square-root equation in offset-midpoint coordinates. First migrating the *CMP* data (assuming zero or constant dip) using the velocity estimate $\bar{v}(z)$. Next reversing the process, but using a constant velocity $\hat{v}$ for diffraction. We follow this approach, but using ray-tracing equations instead of the wave equation.

Transformation equations

For a fast implementation of the process, it is convenient to pose the problem slightly different from how it was discussed above. We can think of the deformation process as two transformations applied in a row. First we take the seismic *CMP* gather and determine a velocity function $\bar{v}(z)$. This velocity function does not need to be extremely accurate, but should include the most predictable changes in the velocity function, such as the sea-floor sediment interface for marine data. Using this velocity function we use the ray tracing equations to transform the data into (p,z) coordinates.

$$\begin{bmatrix} t \\ h \end{bmatrix} = \begin{bmatrix} \int_0^z \frac{2\,v(\xi)}{\left[1 - p^2 v(\xi)^2\right]^{1/2}} d\xi \\ \int_0^z \frac{p v(\xi)}{\left[1 - p^2 v(\xi)^2\right]^{1/2}} d\xi \end{bmatrix} \tag{1}$$

where t is two-way traveltime, h is half-offset, v is velocity, and p is the Snell parameter.

If the transformation to (p,z) was done with the exact stratified velocity function, then precritical reflection events should appear straight, independent of p. And the postcritical reflections and refractions should interfere giving a $p-z$ image. This image has been used by Clayton and McMechan to determine velocity from refraction data. (Clayton and McMechan, 1980, SEP-24, p. 33-56; Clayton, 1980, SEP-27).

The second step is to take the data from the (p,z) space into new *CDP* $(\hat{h},\hat{t})$ coordinates. This second transformation is done at a constant velocity $\hat{v}$. For constant velocity we can invert the ray-equations (1) to get

$$\begin{bmatrix} p \\ z \end{bmatrix} = \begin{bmatrix} \frac{\hat{h}}{\hat{v}^2 \hat{t}} \\ \frac{1}{2}\left(\hat{v}^2\hat{t}^2 - \hat{h}^2\right)^{1/2} \end{bmatrix} \tag{2}$$

Now if the initial $\bar{v}(z)$ was correct, reflection events should all appear hyperbolic. Figure (1) summarizes the transformations.

For computation the intermediate step is not necessary. Since the ray equations are invertible for the second transformation, we may substitute directly equation (2) into (1) to get the result in a single pass. The algorithm is:

```
for all ĥ
    for all t̂
        solve (2) for (p,z)
        solve (1) for (h(p,z),t(p,z))
        P̂(ĥ,t̂) = P(h,t)
    end
end
```

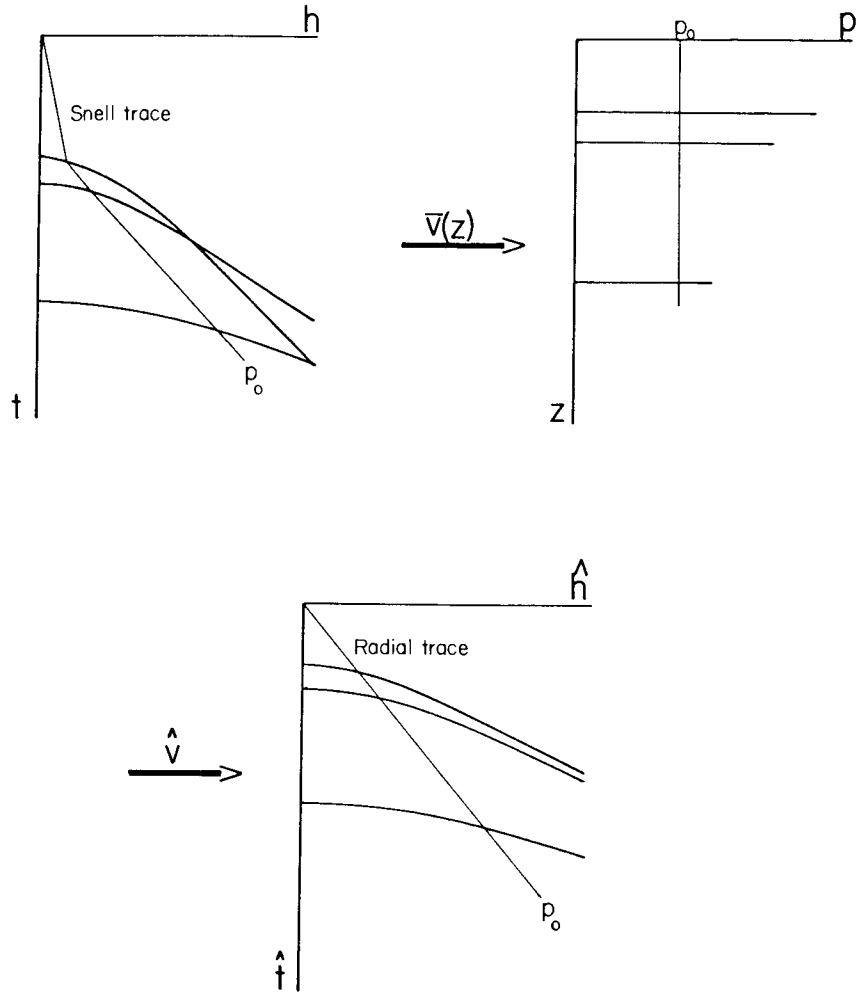

FIG. 1. Deformation of a *CMP* gather with $\bar{v}(z)$ to hyperbolas.

Velocity analysis

After application of the deformation process, if the starting velocity function was exact, all events should align along the inverse mapping velocity $\hat{v}$ in the velocity-spectrum. Errors in the velocity function appear as departures from $\hat{v}$. As a first order correction we can use the ratio between the observed velocity for a fixed reflection event and $\hat{v}$ to correct its RMS velocity. We think this correction should be sufficient. Otherwise we may iterate the process. For the first pass, we can use the estimated $\bar{v}(z)$ from the conventional velocity-spectrum, and then enhance resolution applying the hyperbolic deformation with this velocity function.

Synthetic data examples

Figure (2) shows the synthetic model computed using ray-tracing equations. The model has a thin high-velocity layer just below the sea bottom. It is for this case that we expect our deformation process to be the most useful. In this figure we also display the computed velocity-spectrum. The velocities are in a $2:1.2:1$ ratio, the arrival times are $1:1.25:2.22$ of t_0.

Note in particular the poor resolution for the second arrival. We will concentrate our attention in this event. The third arrival has a narrow range of p parameters, therefore it is quasi-hyperbolic, and we do not hope to resolve it much further.

In figure (3) we plot the transformed data into (p,z) coordinates. In figure (3a) we used the correct velocity model. As expected the arrivals do appear straight, independent of p. The noisy energy that occurs in the gather for large p values comes from the postcritical angle arrivals, this energy plus refraction energy interferes constructively to give a (p,z)-image. In figure (3b) the velocity function included water velocity and the first sediment velocity. Now, for the third event we notice a pull-up because underestimation of its velocity. In figure (3c) we overestimated the bottom layer interval velocity by 16%, what we get is a pull-down effect. Figure (3d) shows the data obtained when we do the mapping using the velocities obtained with conventional velocity estimation. As expected, the difference between figure (3a) and figure (3d) is emphasized for high p-values.

In figure (4) we consider the problem of resampling the data. For this purpose the forward model $\bar{v}(z)$ was exact. The problem with stretching algorithms is that early and late arrivals are stretched differentially. depending on the mapping velocities. Figure (4a) shows the effect of mapping with a slow inverse $\hat{v}$ velocity. The figure has an offset interval half the original, the timing interval is the same. A slow velocity stretches too much late arrivals, then we are forced to resample more densely the data, without increasing its

information. This is not a good choice for doing the mapping. The velocity-spectrum is shown in figure (4b), note all events align along water velocity. Figure (4c) was computed with $\hat{v} = 2500 m/s$. The sampling was not modified from the original data. The velocity-spectrum is shown in figure (4d). Here we are undersampling the first sea-floor reflection arrival, this arrival is however not crucial to our discussion. The third arrival is still oversampled. Finally in figure (4e) we used the fastest velocity in the inverse mapping. Now both the first and second arrival are undersampled. The advantage of this velocity is that we have most of the original information in the new gather. The velocity-spectrum is shown in figure (4f). Note first that even thou we undersampled the first event, its velocity is still sharply defined. Also the resolution of the second event has been enhanced as expected, compare with the velocity-spectrum of the original data in figure (2b).

In the next figure (5) we applied the process when the velocity model $\bar{v}(z)$ was taken from conventional velocity estimation. Figure (5a) shows the data after deformation using $\hat{v} = 2500 m/s$. The quality of the second event has been enhanced noticeable. Also this event now appears at lower velocity than expected, this effect because hyperbolic velocity estimators overestimate the velocity function in stratified media. We can check from this figure that the departure from the expected $\hat{v}$ gives almost the exact RMS velocity for the event (< 5% error).

Figures (6) and (7) were computed underestimating and overestimating the velocity of the third layer. (16.6% error in both cases). The inverse velocity was $\hat{v} = 3000\ m/s$. The reader may verify that the velocity correction implied in the spectrum gives an accurate factor to update the initial velocity model.

Field data examples

Figure (8a) shows the field data used to try out the method. In figure (8b) we display the conventional velocity-spectrum. There is a discontinuity in the RMS velocity function from the sea floor arrival in the sediments below of 1.5 water velocity, at ~1.5 s. We try to increase the resolution of the velocity-spectrum in this interval.

In figure (9) we display the data in the (p,z) domain. (In the implementation of the method we did all the transformations directly from (h,t)-space to $(\hat{h},\hat{t})$-space). The velocity function $\bar{v}(z)$ was taken from the conventional velocity-spectrum, however only two velocities were included: water velocity down to 720 m, and a sediment velocity of 2500 m/s below; p ranges from 0 s/m to 1/2130 s/m. The range of depths is from surface to 6250 m. Water arrivals have straighten as expected, and later reflections are curved upwards because velocity underestimation.

Figure (10) was computed using the same velocity function as in the previous figure. The inverse velocity $\hat{v} = 2500\ m/s$. Now the water layer was replaced by sediment velocity. Pay particular attention to the events in the range $1 - 1.6\ s$ in the original velocity-spectrum, now in the range $.6 - 1.2\ s$. Events in this range are more resolvable after stretching, therefore it should be easier to discriminate primaries from multipes, and obtain a more accurate and detailed velocity function in this range.

Figure (11) was computed with a different forward velocity model $\bar{v}(z)$. The sea-floor was put at 480 m, with a constant velocity of 2500 m/s below. The inverse velocity was $\hat{v} = 2500\ m/s$. The range $1 - 1.6\ s$ in the original velocity-spectrum has been transformed to the range $.74 - 1.34\ s$.

To compare the velocity-spectrums look for instance at the event at 1.424 s in the original spectrum (figure 8b). This event has been moved to 1.04 s in figure (10) and to 1.168 s in figure (11). It is apparent that its resolution has been enhanced Also multiple reflections are more apparent in the velocity-spectrum of the deformed gathers, this way it becomes easier to identify them and avoid confusing them as primary reflections.

Conclusions

From our examples we think that the proposed hyperbolic deformation has an excellent potential as part of routine processing for velocity estimation, in particular in areas when we have wide-offsets and a hard sea-floor. The method requires an estimate for $\bar{v}(z)$, which we showed can be taken from a first-pass conventional velocity estimation. The deformation is fast, with negligible cost. The main cost will be the need to repeat the velocity estimation after stretch, with the advantage that no special programs are required. This cost is less or comparable with other alternatives to non-hyperbolic velocity estimators.

ACKNOWLEDGMENTS

We gratefully acknowledge Rick Ottolini who wrote the velocity estimation program we used in this paper.

REFERENCES

Bruce T.M., and Straley, D.K., 1979, Higher-order moveout spectra: Geophysics, v 44, p. 1193-1207.

Taner, M.T., and Koehler, F., 1969, Velocity spectra - digital computer derivation and application of velocity functions: Geophysics, v 34, p. 859-881.

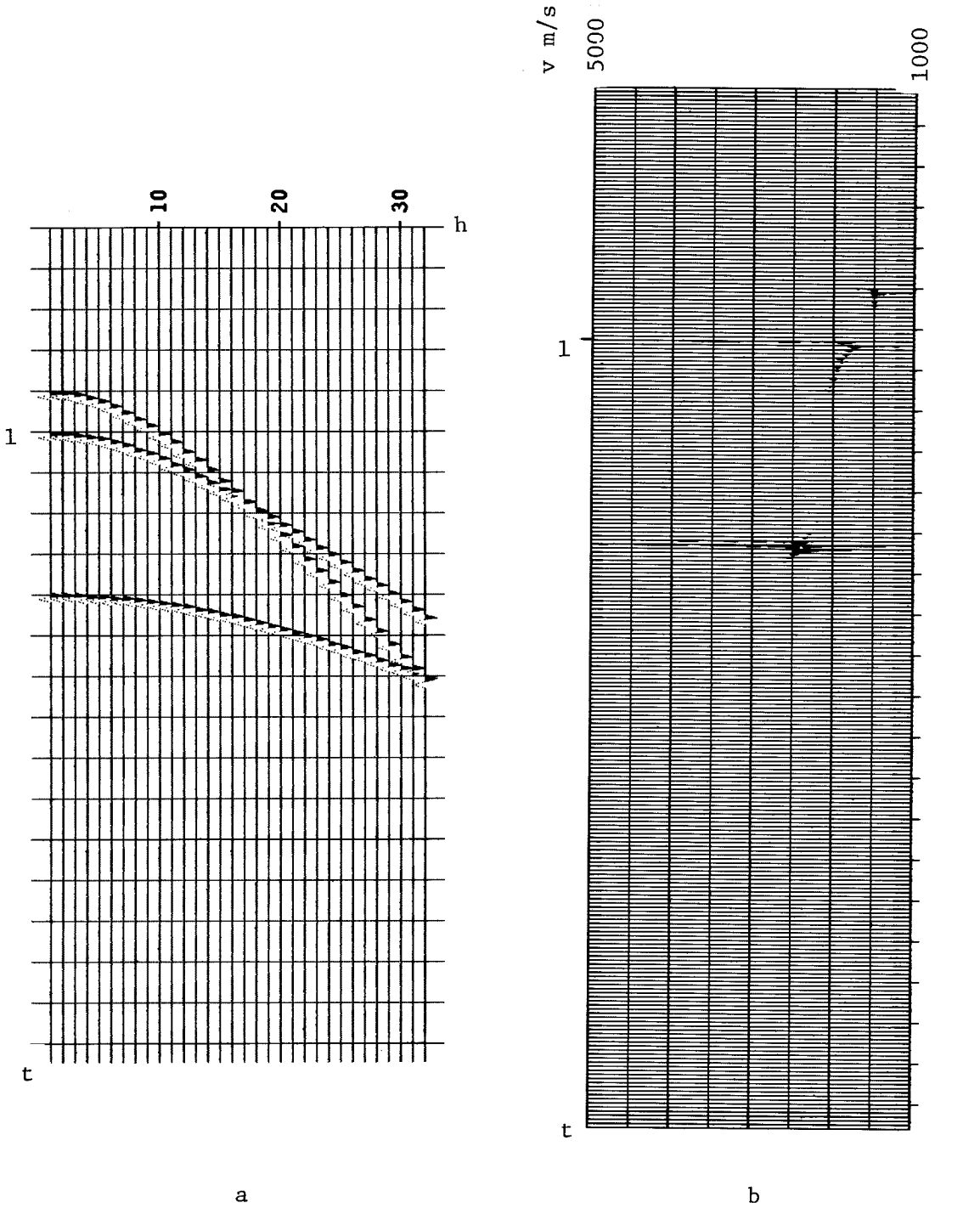

FIG. 2. (a) is a synthetic gather. There are 32 traces with 512 time samples. dh = 50 m, dt = .008 s. The arrival times are (.8,1.0,1.776) s, the velocities (1500,2500,3000) m/s. (b) is the conventional velocity-spectrum. Sampling is dt = 0.016 s. Note in particular the poor resolution for the second arrival.

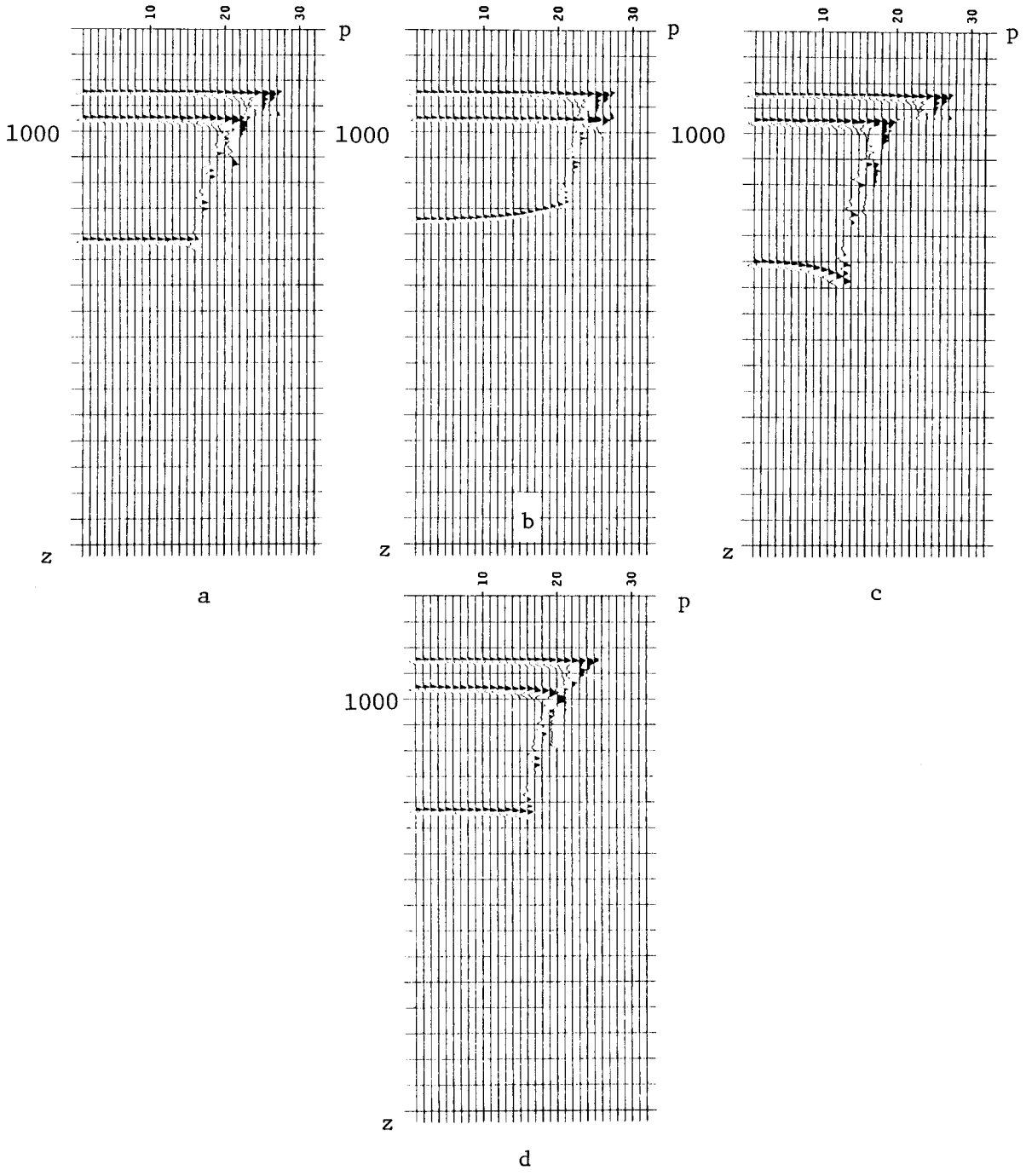

FIG. 3. This figure shows the transformation of the data to (p,z)-space. In (a) we used the correct velocities, the three arrivals look straight for precritical arrivals. In (b) we underestimated (16%) the velocity for the third layer, this changes the depth coordinate of the event, and the event shows a pull-up effect analogous to undermigration. In (c) we overestimated the third layer velocity (16%), the effect is one of overmigration. In (d) we used the velocity function from conventional velocity analysis, the main effect is for high p values in the second arrival. In this figure dp = 1.0e−5, dz = 10 m. In this and all figures linear interpolation was used.

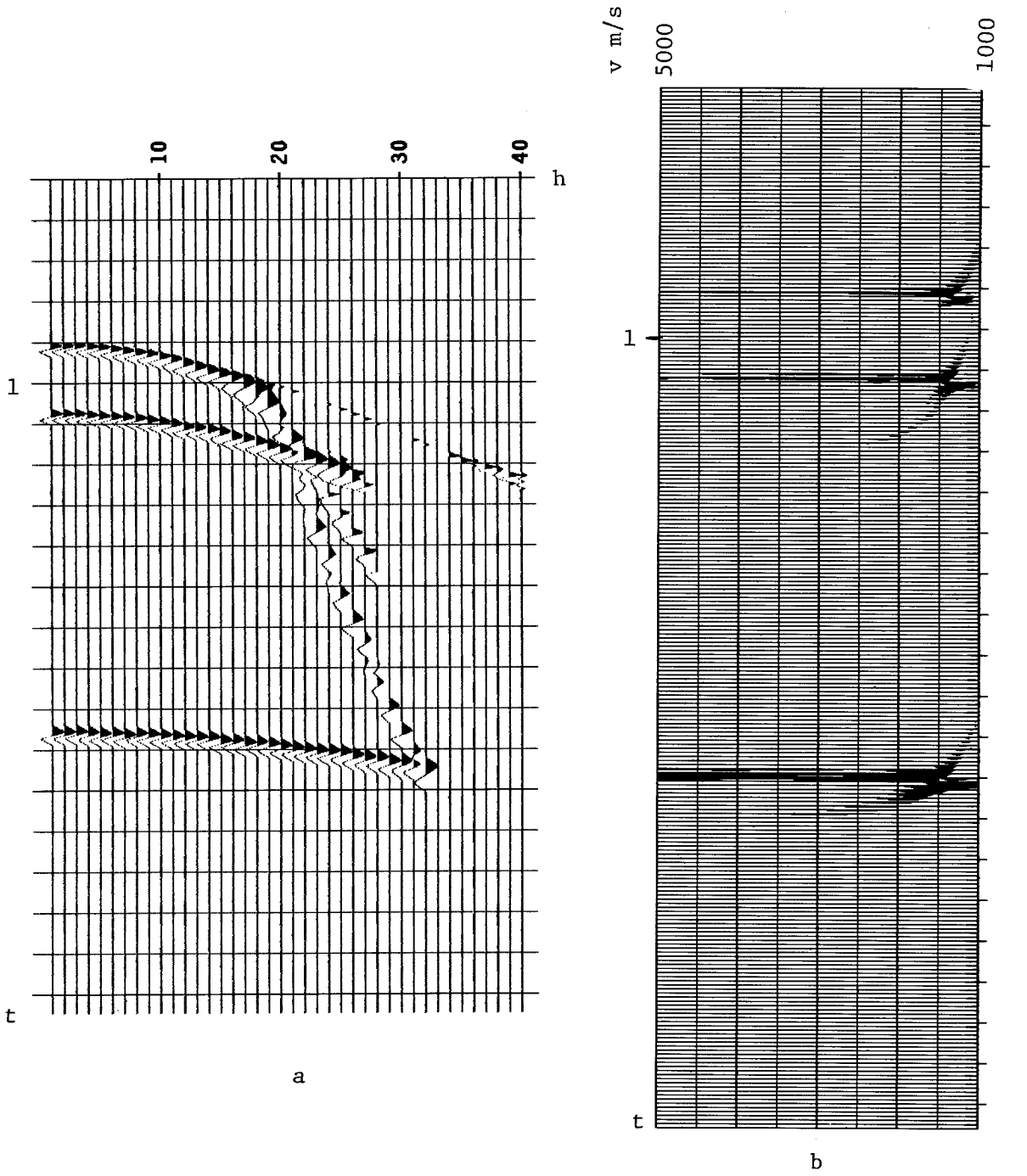

FIG. 4a,b. Figure (a) shows the transformation into $(\hat{h},\hat{t})$ coordinates. The forward velocity is exact. The inverse velocity is $\hat{v}$ = 1500 m/s. We modified the offset interval to dh = 25 m. With this low velocity we are oversampling the second and third arrivals. The noise in the figure comes from the nonuniqueness of p, *ie*, for a fixed p we can have energy at a given offset from several t_0 events. The velocity-spectrum (b) shows as expected the arrivals aligned along $\hat{v}$.

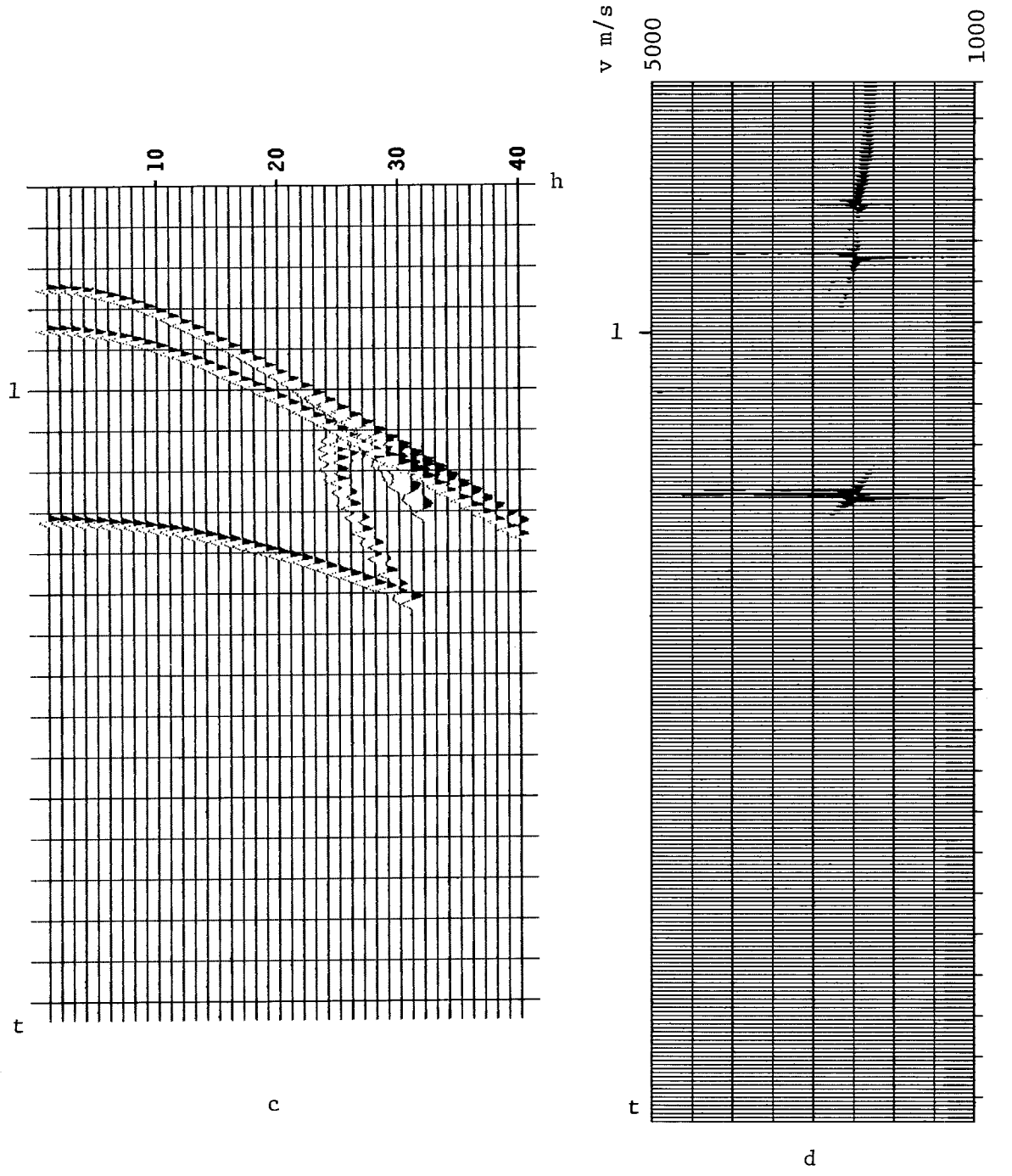

FIG. 4c,d. In figure (c) we changed the inverse velocity to $\hat{v}$ = 2500 m/s. Now we are undersampling the first arrival. With this velocity one does not need to change the sampling parameters ($\hat{dh}$,$\hat{dt}$). The velocity-spectrum (d) shows the events aligned along $\hat{v}$. Note in particular the improvement of resolution for the second event compared to figure (2b).

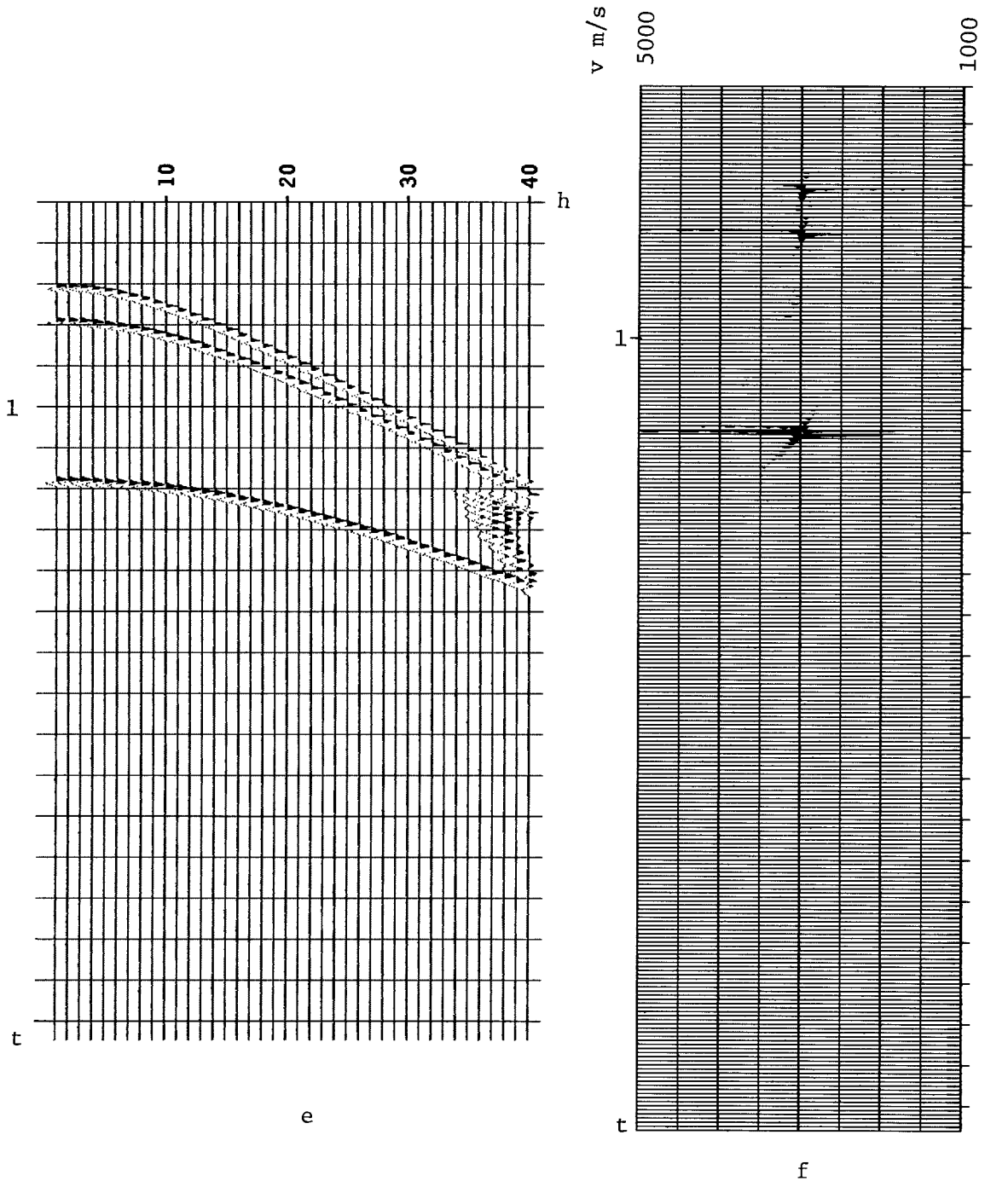

FIG. 4e,f. Figure (e) displays the mapping when $\hat{v}$ = 3000 m/s. This velocity will be used in following figures. The sampling parameters have not been changed. Figure (f) shows the velocity-spectrum. Again compare the resolution of the second arrival with figure (2b).

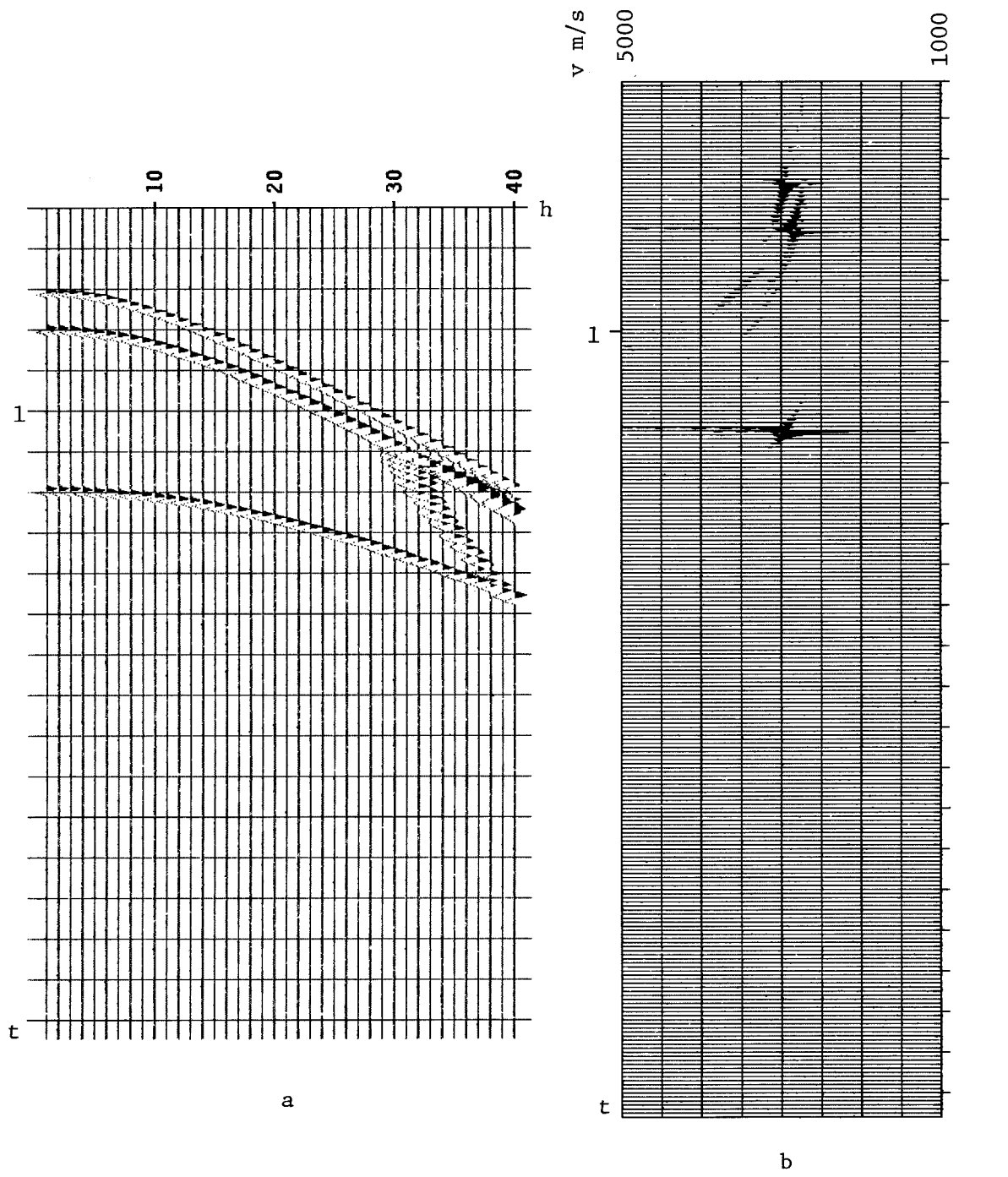

FIG. 5. In this figure we show the implementation of the transformation when the forward $\bar{v}(z)$ is taken from the conventional velocity-spectrum of figure (2b). Figure (a) displays the data after transformation, we added traces to include as much of the original data as possible. Sampling parameters are not changed. Figure (b) shows the velocity-spectrum. Compare the resolution of the second event. Now we have an error because conventional analysis overestimates the velocity function. This causes the misalignment observed in the figure. The relative displacement of the observed and expected velocities gives the correction to the forward RMS velocity.

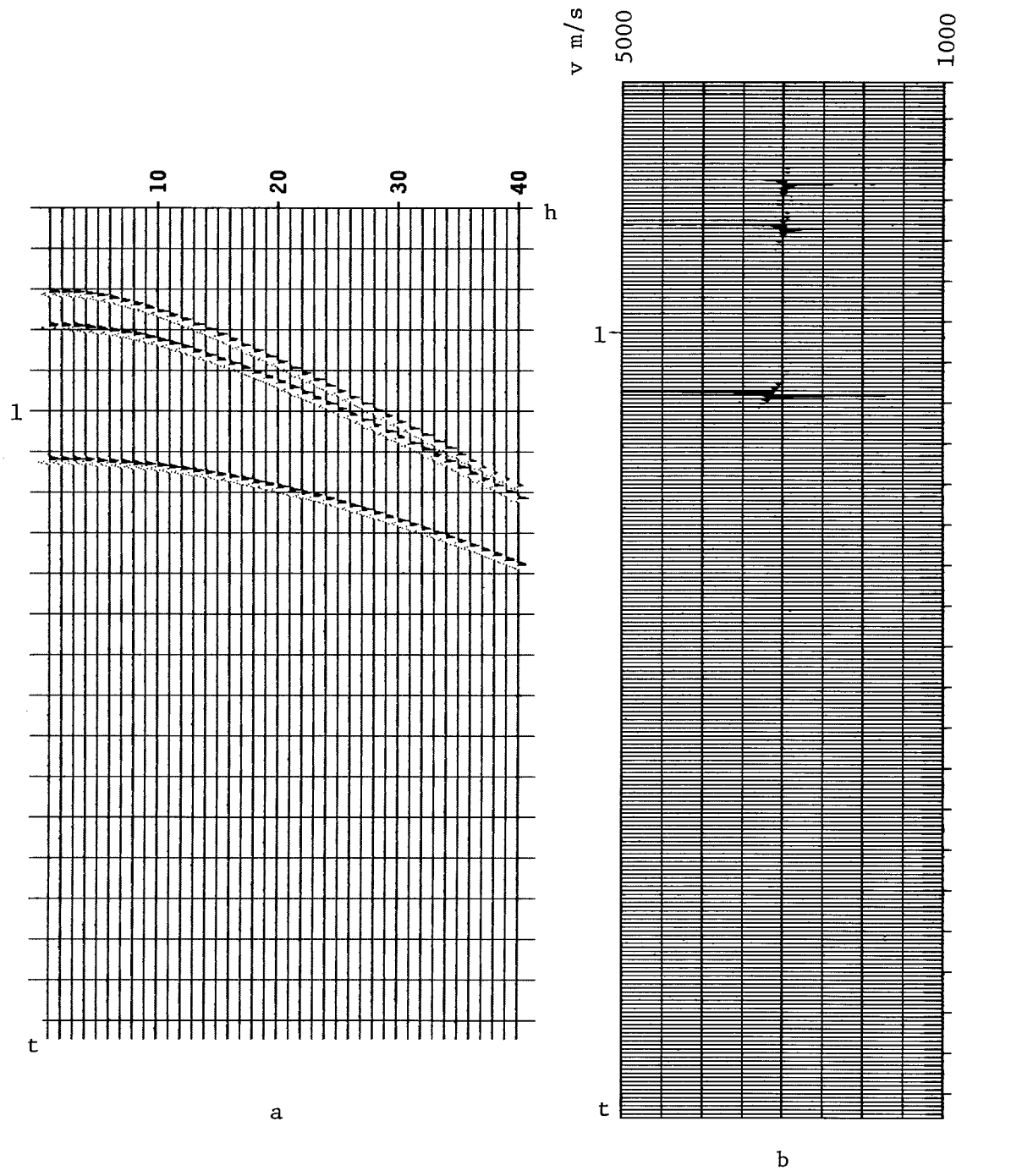

FIG. 6. In this figure we underestimated the third velocity layer. We try to see the sensitivity of the method to errors in the forward velocity model $\bar{v}(z)$. Only the first and second arrival velocities were used. The resolution of the velocity-spectrum is still sharper than in figure (2b). The departure from the expected $\hat{v}$ = 3000 m/s gives the right factor to correct for the underestimated velocity of the third event.

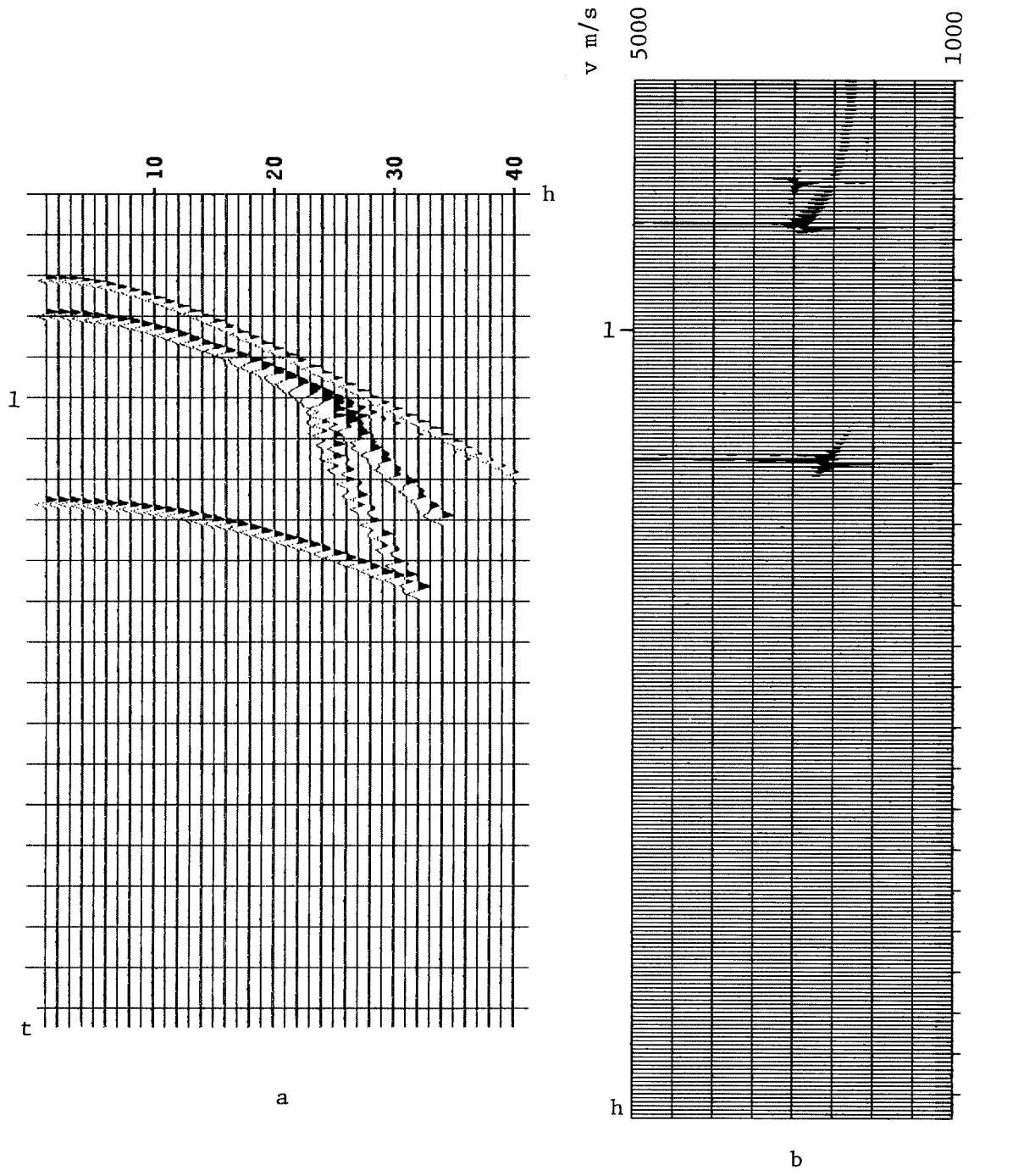

FIG. 7. This figure is analogous to figure (6), but here we overestimated the third velocity layer by (16%) in the forward $\bar{v}(z)$. Again the correction implied by the spectrum is enough to get an almost exact RMS velocity (within 5%).

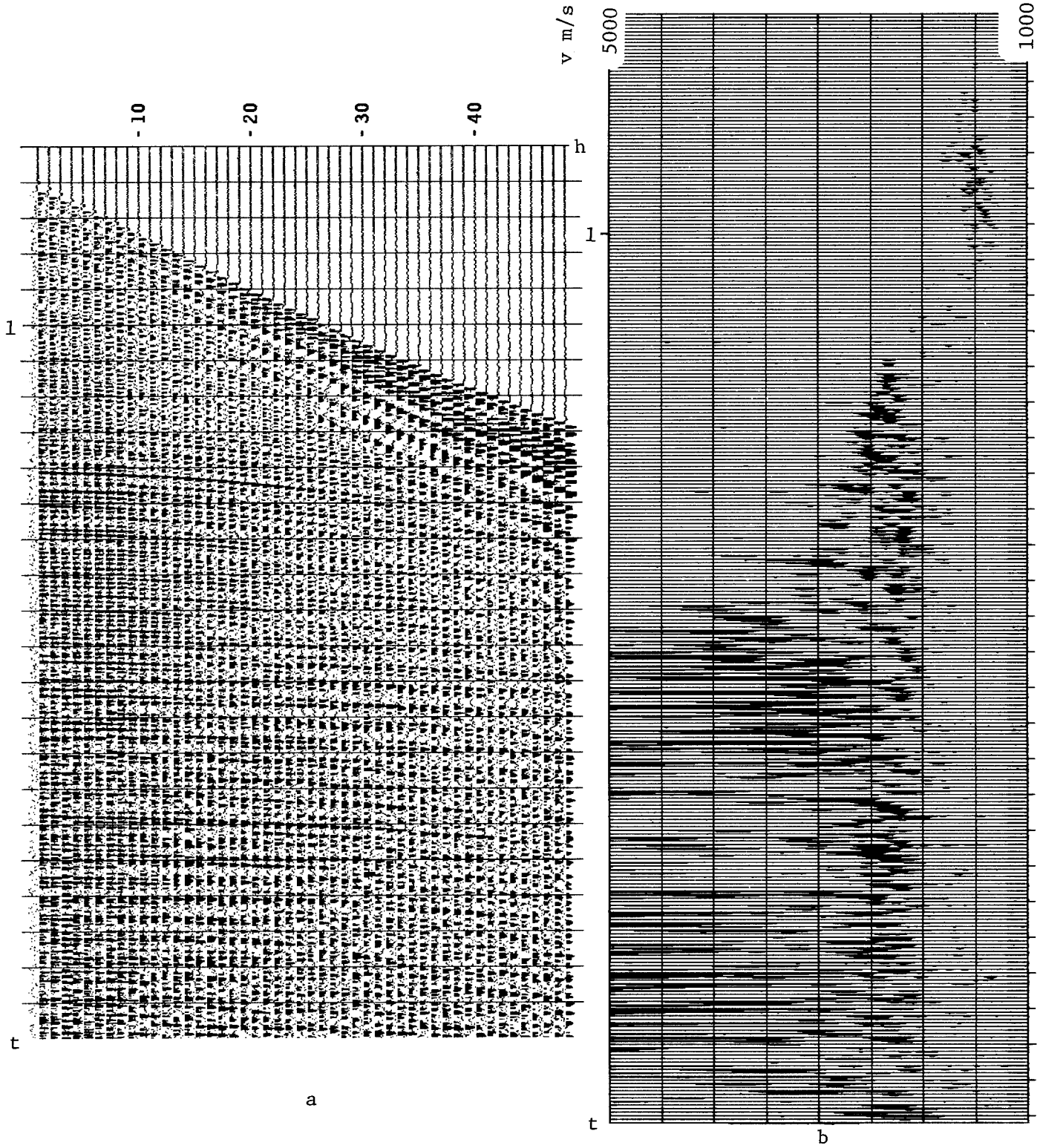

FIG. 8. (a) is the data gather used for the field data examples. The gather has an *square−root* gain applied. There are 48 traces and 1250 time samples, $df = 50\ m$ (full offset), $dt = 0.004\ s$. The near trace is 262 m. (b) displays the conventional velocity-spectrum. Note in particular the poor resolution for events between $1 - 1.6\ s$. Follow the event at 1.424 s for comparison with the transformed results.

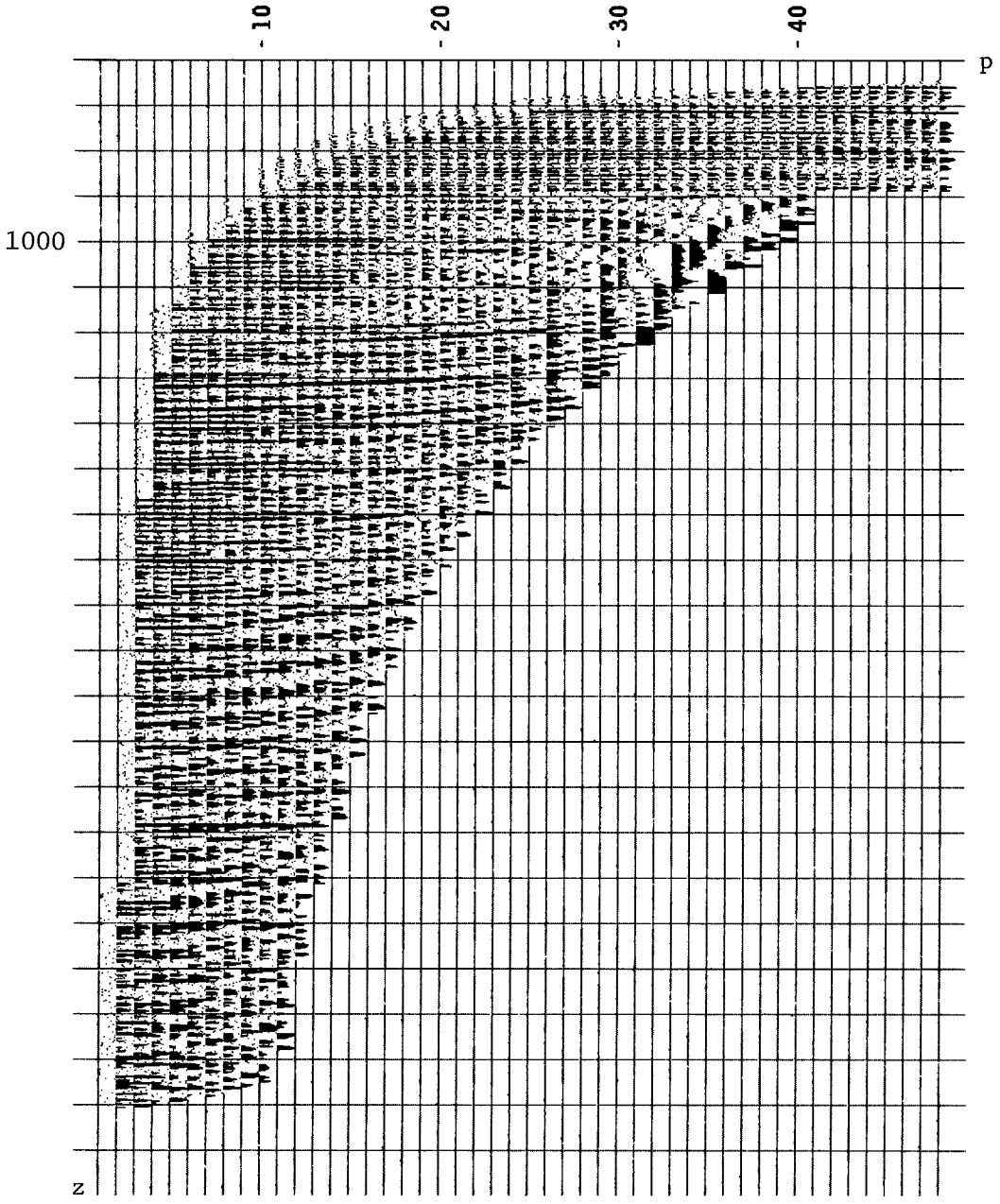

FIG. 9. In this figure we display the data in the (p,z) domain. The velocity function is a water layer 720 m deep overlying a constant velocity half space (2500 m/s). dz = 5 m, dp = 1.0e −5. Note that the sea-floor arrival is straight as expected, and below primaries curved up because too small velocity, while multiples curve down because too fast velocity.

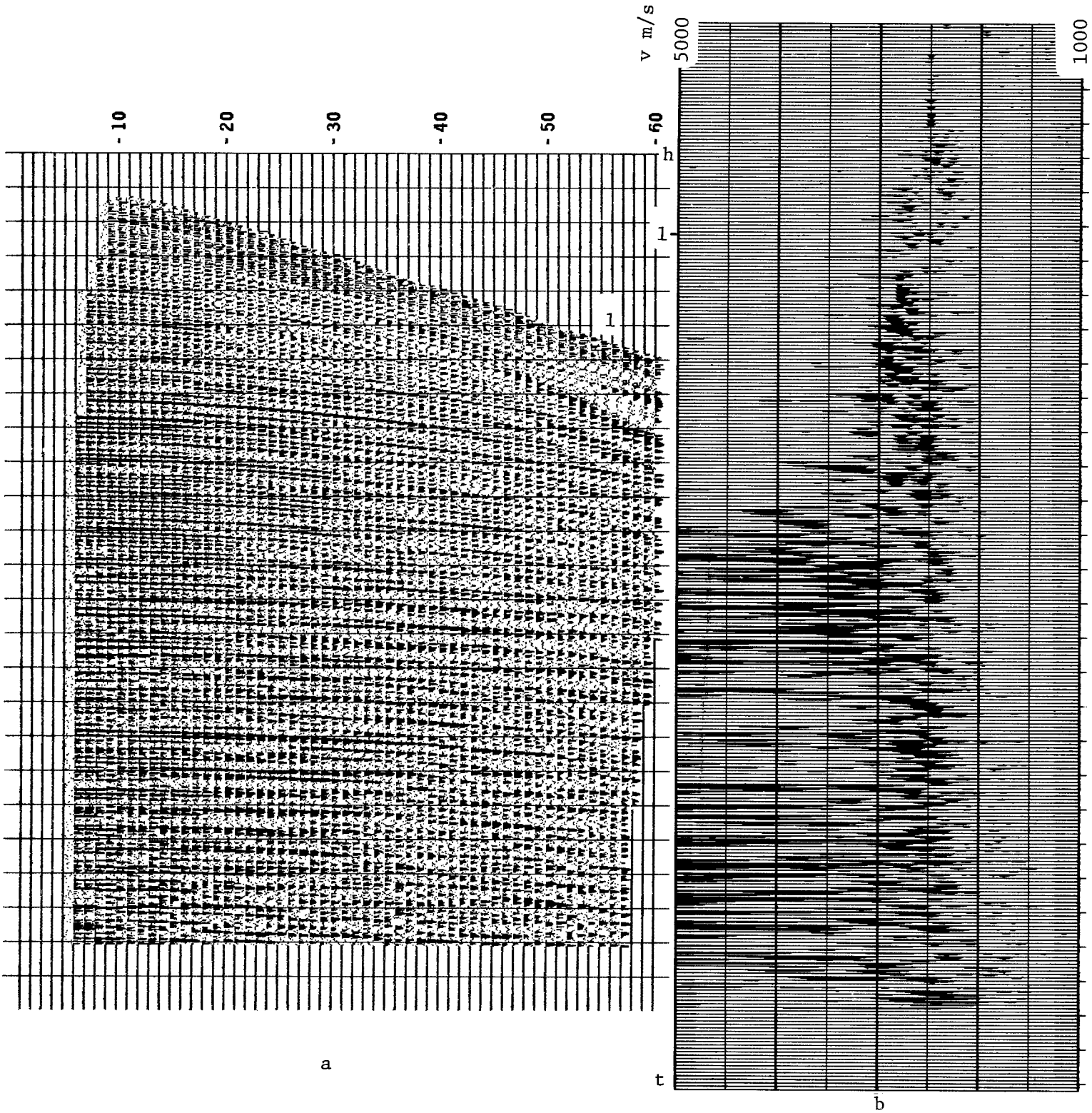

FIG. 10. In this figure we used the same forward velocity model defined in figure (9). The inverse velocity is $\hat{v}$ = 2500 m/s. We added up to 60 traces to keep from losing information in the transformation. (b) is the velocity-spectrum. Compare the arrivals between 0.6 – 1.2 s with figure (8b). The reference event is now at 1.04 s.

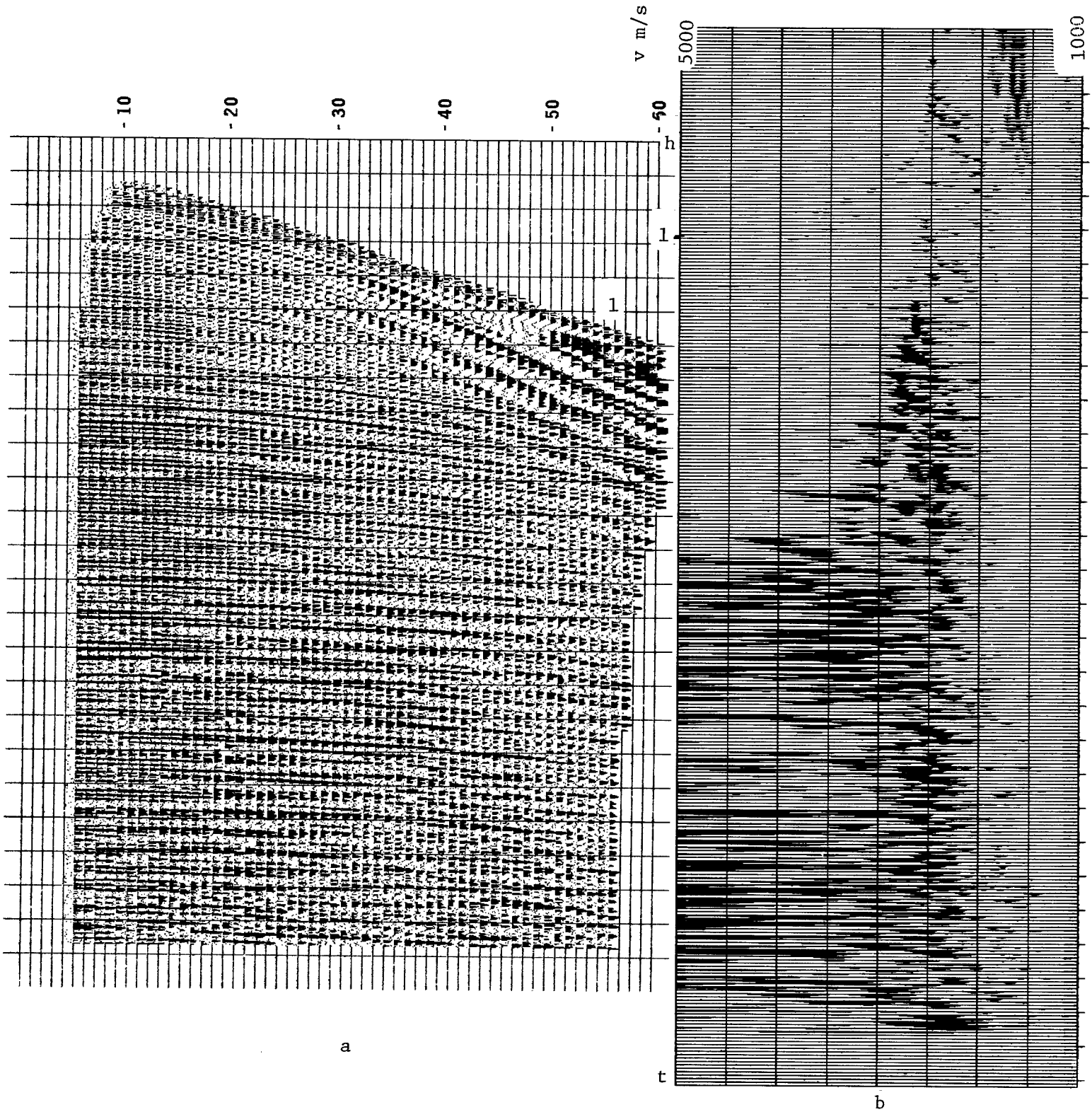

FIG. 11. In this figure we still used two velocities, but changed the sea-bottom to 480 m. The reference range is now .74 – 1.34 s and the reference event is at 1.168 s. The resolution is not changed considerably, implying that the method should work with a rough guess of $\bar{v}(z)$.